Gas Permeability Properties of Polysulfone Membranes Containing the Mesoporous Molecular Sieve MCM-41

Brian D. Reid, F. Alberto Ruiz-Trevino, Inga H. Musselman,*
Kenneth J. Balkus, Jr., and John P. Ferraris

Department of Chemistry, The University of Texas at Dallas, P.O. Box 830688, Richardson, Texas 75083-0688

Received November 28, 2000. Revised Manuscript Received April 11, 2001

In this study, we have explored the first use of the siliceous MCM-41 molecular sieve as an additive to enhance the gas permeability characteristics of a high-performance polysulfone. For all gases tested (N_2, O_2, CO_2, CH_4), the permeability increased in proportion to the weight percent of MCM-41 present in the film. At the same time, calculated ideal selectivities remained almost constant irrespective of MCM-41 loading. ATR-FTIR spectroscopy, supported by molecular mechanics calculations, revealed hydrogen-bonding interactions between polysulfone and MCM-41. The increase in permeability, without a loss in selectivity, which is not observed with dense silica or zeolites, suggests that using a mesoporous molecular sieve as the adsorbent additive enhances contact and penetration of the polymer.

Introduction

To enhance the gas permeability and selectivity properties of conventional polymeric membranes, the incorporation of various nanoporous materials, such as zeolites and carbon molecular sieves, into a polymer matrix has been investigated.[1] The primary motivation for preparing such mixed-matrix composites is to join the microporous or nanoporous material adsorption and sieving properties and the polymer processability. However, such composites often result in only moderate increases in permeability with corresponding decreases in selectivity for gas pairs of industrial significance.[2] The poor performance of zeolite/polymer composites may result from inadequate wetting and aggregation of the microporous zeolite particles within the polymer matrix. Weak interactions between a dense polymer matrix and a microporous zeolite additive may lead to the formation of nonselective channels or voids within the membrane, resulting in Knudsen flow.

Mesoporous materials possess pores large enough (20−300 Å) to readily allow the penetration of polymer chains, resulting in better wetting and dispersion. Recent molecular dynamics simulations of gas permeation through polyethylene confined between graphite planes separated by 57 Å imply that polymers confined in mesoporous media may exhibit some improvement in selectivity coefficients.[3] In addition, an increase in oxygen permeability along with an increase in O_2/N_2 selectivity has been reported for polymer/silica composites supported on an Anopore ceramic support with 100−300 Å pores.[4]

A class of mesoporous molecular sieves was recently developed by Mobil utilizing charged surfactant templates.[5,6] MCM-41 (Mobil Composition of Matter-41) is a hexagonal member of this family which has tremendous potential for mixed-matrix gas separation membranes. MCM-41 possesses well-ordered one-dimensional pores that run in parallel (Figure 1a). It is typically formed by the condensation of silica around self-assembled arrays of surfactant molecules in an aqueous gel. In addition to its larger pore size, MCM-41 is unique from other adsorptive additives in its compositional and morphological flexibility. For example, the hydrophilicity of MCM-41 may be modified through control of the Si/Al ratio. In addition, other transition metal oxides or aluminophosphates may be used to prepare MCM-41 type materials. The siliceous mesophases may also be prepared with a variety of particle shapes including hexagons, spheres, gyroids, rods, and tubules.[7] Also, the pore size may be varied from 20 to 300 Å depending on the template used during synthesis. The internal surface of the MCM-41 mesopores is decorated with hydroxyl groups, which may be derivatized in order to introduce other selectivity enhancing functional groups.

In this study, the siliceous MCM-41 was evaluated as an additive to enhance the gas permeability characteristics of the high-performance polysulfone (PSF) polymer. Although size and shape selectivity are not expected with small molecules, recent work has shown significantly higher adsorption for CO_2 than CH_4 on siliceous MCM-41.[8] PSF was selected as the support matrix because its permeability−selectivity combination falls close to Robeson's "upper bound" region.[9] Addition-

* Corresponding author.

(1) Zimmerman, C. M.; Singh, A.; Koros, W. J. *J. Membr. Sci.* **1997**, *137*, 145 and references therein.
(2) For example: Gur, T. M. *J. Membr. Sci.* **1994**, *93*, 283.
(3) Rallabandi, P. S.; Ford, D. M. *J. Membr. Sci.* **2000**, *171*, 239.
(4) Moaddeb, M.; Koros, W. J. *J. Membr. Sci.* **1997**, *125*, 143.
(5) Kresge, C. T.; Leonowicz, M. E.; Roth, W. J.; Vartulli, J. C.; Beck, J. S. *Nature* **1992**, *359*, 710.
(6) Beck, J. S.; Vartulli, J. C.; Roth, W. J.; Leonowicz, M. E.; Kresge, C. T.; Schmitt, K. D.; Chu, C. T.-W.; Olson, D. H.; Sheppard, E. W.; McCullen, S. B.; Higgins, J. B.; Schlenker, J. L. *J. Am. Chem. Soc.* **1992**, *114*, 10834.
(7) Coombs, N.; Khushalani, D.; Oliver, S.; Ozin, G. A.; Shen, G. C.; Sodolov, I.; Yang, H. *J. Chem. Soc., Dalton Trans.* **1997**, *21*, 3941.

10.1021/cm000931+ CCC: $20.00
Published on Web 06/16/2001

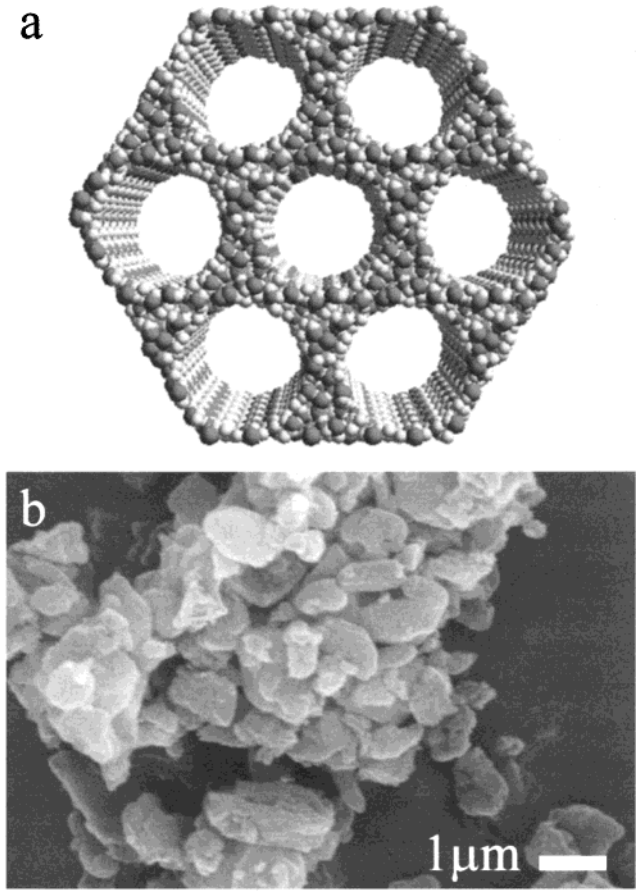

Figure 1. (a) Structural model of the 1-dimensional mesoporous structure of MCM-41 (pore diameter = 40 Å) and (b) an SEM image of MCM-41.

ally, PSF and the structurally similar polyethersulfone (PES) have been used previously as matrix materials for zeolite composite membranes.[2,10−12] The results of these studies can be compared with those of MCM-41/PSF composite membranes. The preparation and characterization of MCM-41/PSF composite membranes is described for several MCM-41 loadings. Additionally, the permeabilities of N_2, O_2, CH_4, and CO_2 in the composites at 35 °C were determined. Results indicate that the MCM-41 additive serves to enhance the diffusivity and overall permeability of the small molecules without a loss of selectivity.

Experimental Section

Materials. The UDEL P-1700 (polysulfone, MW = 65 000−70 000 g/mol) was obtained from Amoco. Materials for MCM-41 preparation, including sodium silicate and cetyltrimethylammonium bromide (CTAB), were obtained from Aldrich and used as received. Fumed silica (99.8% pure) used in silica/PSF composites was obtained from Aldrich and used as received. Gas permeation experiments were conducted using 99.99% pure O_2, N_2, and CO_2 and 93% pure CH_4 (BOC, impurities unknown).

Instrumentation. SEM images were acquired using a Philips XL30 scanning electron microscope. Samples for SEM analysis were prepared using a Denton Vacuum Desk II sputter coater with a gold−palladium target. XRD patterns were obtained with a Scintag XDS 2000 X-ray diffractometer using Cu Kα X-radiation. IR spectra (1000 scans, 1 cm^{-1} resolution) were collected using a Nicolet Avatar 360 FTIR E.S.P. spectrophotometer equipped with a single-bounce attenuated total reflectance (ATR) accessory.

Preparation of MCM-41. CTAB was used as a template to obtain a 4 nm pore size using published procedures.[13] In a Teflon bottle, 2.53 g of sodium silicate was stirred in 6.43 g of deionized water for 40 min, followed by the addition of 0.16 g of concentrated H_2SO_4 (95−98%) with 30 min of further stirring at room temperature. At the same time, 2.19 g of CTAB was dissolved in 7.919 g of deionized water and stirred for 40 min. Next, the CTAB solution was added to the sodium silicate solution; the mixture was stirred for 1 h. The synthesis gel was heated at 100 °C for 5 days under static conditions. The pH (initially 11.3) was adjusted to between 9 and 10 once per day using 10% H_2SO_4. After removal from the oven, the MCM-41 was washed with approximately 3 L of deionized water and dried at room temperature for 2 h. The siliceous MCM-41 was calcined at 540 °C for 16 h to remove the template. The MCM-41 was characterized by X-ray diffraction, which revealed five reflections (2θ = 2.2, 3.7, 4.3, 5.6, 6.4°). Figure 1b shows a scanning electron micrograph of the calcined material, and it reveals an aggregate of small irregularly shaped particles which measures approximately 8 μm across.

Membrane Formation. A narrow distribution of calcined MCM-41 particle sizes (620−880 nm) (Figure 1b) was obtained through a combination of slow sedimentation and centrifugation of aqueous suspensions. Following these steps, the MCM-41 was vacuum-dried at 120 °C for 2 days. The PSF was dissolved in chloroform to form a 13% (w/w) solution prior to the addition of MCM-41. Mixed-matrix composite membranes were then formed using 10, 20, and 30% (w/w) suspensions of MCM-41 in the PSF solution. Aggregation of MCM-41 particles was a problem in the initial membrane formation experiments. To adequately disperse the MCM-41 particles within the PSF matrix, the suspensions used for the preparation were stirred and sonicated for several 10-min periods until a homogeneous suspension was observed. For a 10% (w/w) MCM-41/PSF composite, a typical preparation consisted of dissolving 0.234 g of PSF in 1 mL of $CHCl_3$ and stirring for 24 h at room temperature. Next, 0.026 g of dried MCM-41 was stirred into the transparent polymer solution to form a white suspension. The suspension was stirred for 10 min and then bath sonicated for 10 min. After five additional iterations of stirring and sonicating, a final 30-min sonication period was completed before casting to remove any trapped air bubbles, which could cause the formation of nonselective pores. 10% (w/w) silica/PSF composites were also prepared using the same procedure.

Membranes were cast in a laminar flow hood (PureAire) onto a glass substrate using an AccuLab Jr. Drawdown casting table with a wire wound rod (AccuLab Jr. #80). Membrane thickness for calculation of gas permeability was determined using optical microscopy. Cross sections were prepared by freeze-fracturing the membranes after several minutes of immersion in liquid N_2. SEM images were acquired from the surfaces and cross sections of the membranes.

Permeability Studies. Single-gas permeabilities were evaluated for O_2, N_2, CO_2, and CH_4 using a custom-built gas permeameter.[14] The permeameter consists of a stainless steel permeation cell which separates an upstream pressure transducer from a downstream pressure transducer (MKS Instruments). This cell exposes a membrane area of 0.5 cm^2 to the gas. All valve actuation and pressure monitoring were conducted using LabView 5.0 software (National Instruments). After evacuating both sides of the membrane for several hours,

(8) Koh, C. A.; Montanari, T.; Nooney, R. I.; Tahir, S. F.; Westacott, R. E. *Langmuir* **1999**, *15*, 6043.
(9) Robeson, L. M. *J. Membr. Sci.* **1991**, *62*, 165.
(10) Battal, T.; Bac, N.; Yilmaz, L. *Sep. Sci. Technol.* **1995**, *30*, 2365.
(11) Duval, J. M.; Kemperman, A. J. B.; Folkers, B.; Mulder, M. H. V.; Desgrandchamps, G.; Smolders, C. A. *J. Appl. Polym. Sci.* **1994**, *54*, 409.
(12) Suer, M. G.; Bac, N.; Yilmaz, L. J. *J. Membr. Sci.* **1994**, *91*, 77.
(13) Edler, K. J.; White, J. W. *Chem. Mater.* **1997**, *9*, 1226.
(14) Washmon, L. L. M.S. Thesis, University of Texas at Dallas, Richardson, TX, 1997.

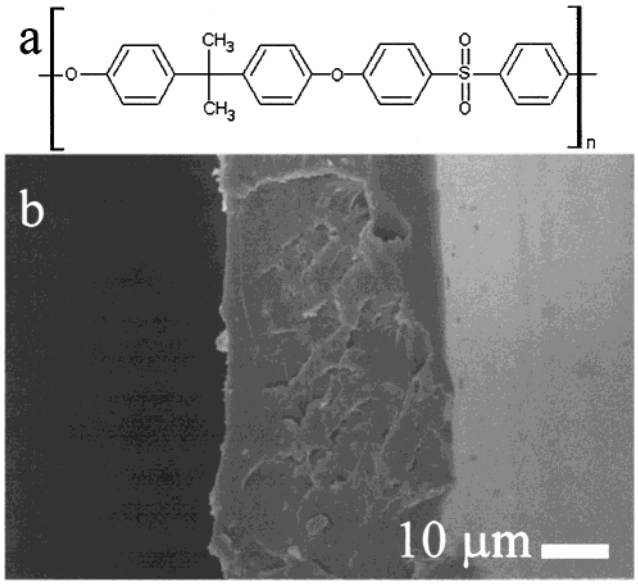

Figure 2. (a) Formula structure of PSF and (b) an SEM image of a PSF membrane cross section.

the upstream side of the membrane was pressurized to approximately 1500 Torr with a single gas. The upstream and downstream pressures were recorded every second for 30 min. The steady-state slope of downstream pressure versus time was determined from the raw data. The time lag (θ, −intercept/slope) and diffusivity (D, L^2/θ) were calculated from the steady-state slope. The permeability was evaluated from 3θ to 7θ, and the solubility was calculated using the equation $S = P/D$. The percent relative error between successive runs for each gas was between 0.2 and 5.6%.

Results and Discussion

Membrane Characterization. UDEL P-1700 PSF (Figure 2a) is a rigid thermoplastic ($T_g = 190$ °C) which is soluble in ketones, aromatic hydrocarbons, and chlorinated hydrocarbons.[15] 13% (w/w) solutions of PSF in $CHCl_3$ form smooth defect-free films upon evaporation. Figure 2b shows the cross section of a pure PSF flat membrane (37.5 μm thick) cast from $CHCl_3$. SEM images of the top side of the pure PSF membrane (not shown) reveal a relatively smooth surface, free from obvious cracks, holes, or other defects.

MCM-41/PSF composite membranes were prepared by dissolving PSF in $CHCl_3$ and adding the appropriate amount of dry MCM-41 followed by repetitive stirring and sonication. Next, the suspension was rod cast onto a glass substrate and dried under vacuum (day 1, 50 °C; day 2, 120 °C; days 3−5, 150 °C; day 6, cooled to room temperature). The extensive stirring and sonication did not alter the crystallinity of the calcined MCM-41. This was verified by suspending MCM-41 in $CHCl_3$ and stirring and sonicating in exactly the same manner as that for the composite suspension. After drying, the stirred and sonicated MCM-41 was examined using SEM which revealed dispersion of large MCM-41 aggregates without any measurable decrease in the individual particle sizes. Also, XRD analysis before and after the stirring/sonication treatment revealed no appreciable reduction in signal intensity or line width for the five reflections (2θ = 2.2, 3.7, 4.3, 5.6, 6.4°) observed for the calcined MCM-41.

(15) Product Data Sheet, Amoco Polymers, Inc., 1999.

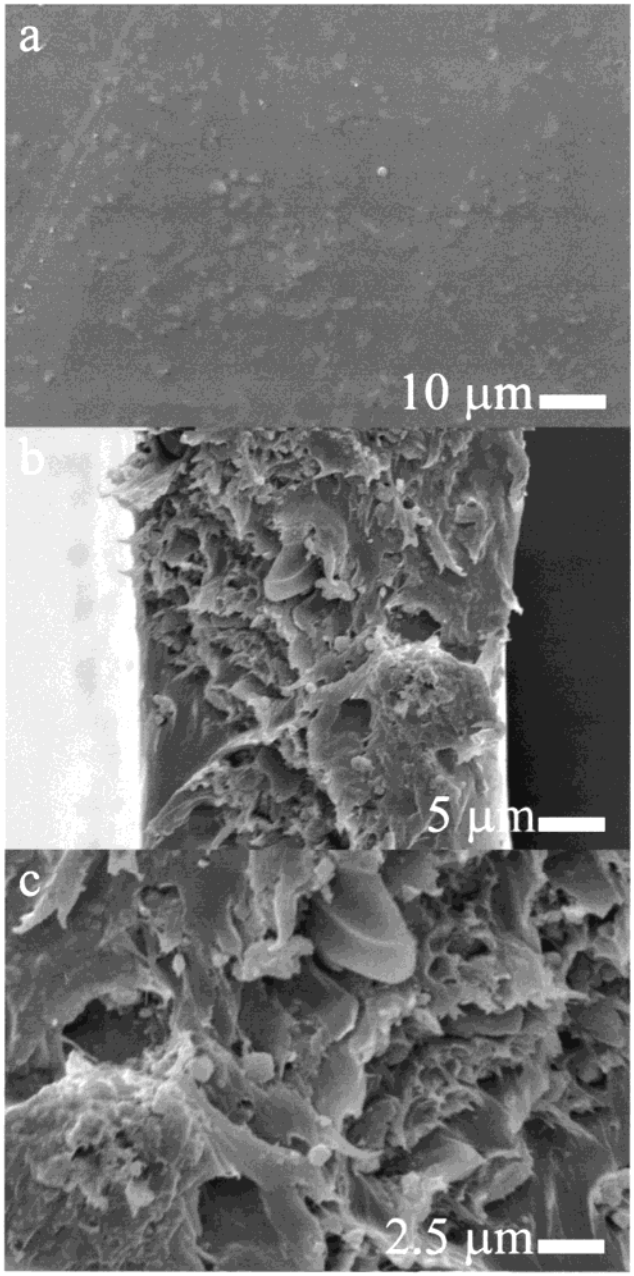

Figure 3. SEM images of a 10% (w/w) MCM-41/PSF composite membrane: (a) top down perspective; (b) cross section; (c) magnified cross section.

The 10 and 20% (w/w) composite films had a cloudy white, semitransparent appearance and were more brittle than the pure PSF membranes. At 30% (w/w) loading, the white membranes became opaque and extremely brittle. Higher loadings of MCM-41 in the composites resulted in membranes that tended to crack under the 1500 Torr pressure on the upstream side of the permeameter. However, control films using as-synthesized MCM-41 (i.e. MCM-41 still filled with the CTAB template) tended to crack even at loadings of 5−10% (w/w) uncalcined MCM-41. Thus, although the MCM-41/PSF composites were more rigid than the pure PSF membranes, penetration of the MCM-41 mesopores by the PSF seemed to impart greater mechanical strength to the composite membranes. Figures 3−5 show top surface (air side) and cross section images of 10, 20, and 30% (w/w) MCM-41/PSF composite mem-

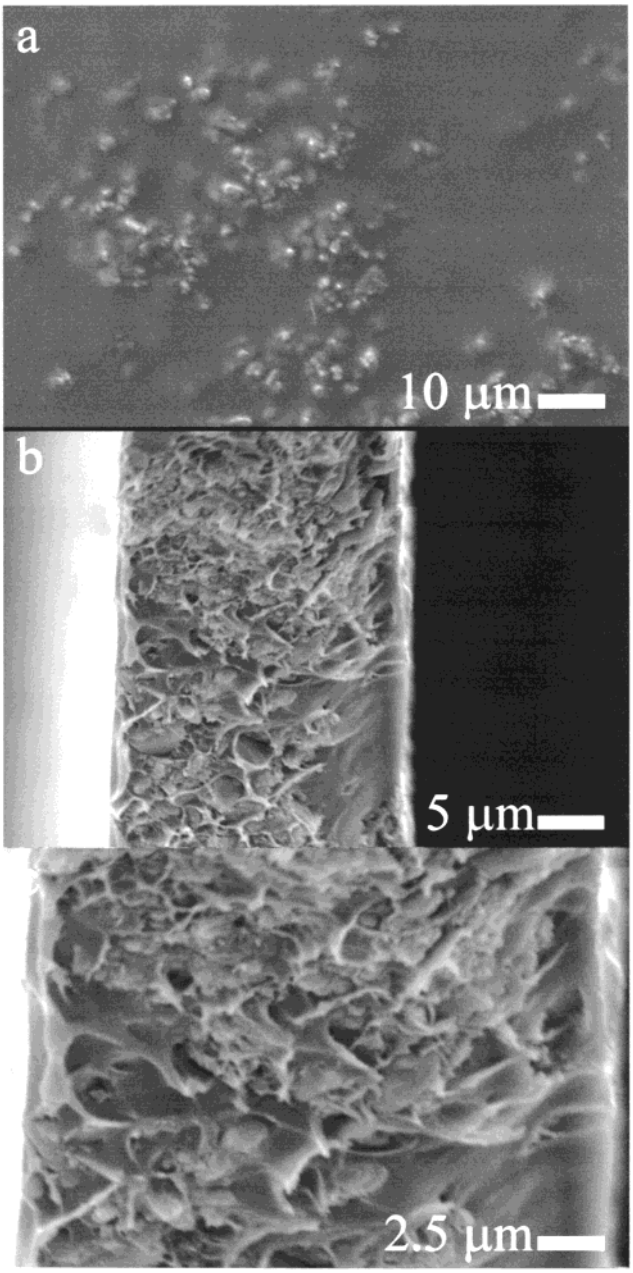

Figure 4. SEM images of a 20% (w/w) MCM-41/PSF composite membrane: (a) top down perspective; (b) cross section; (c) magnified cross section.

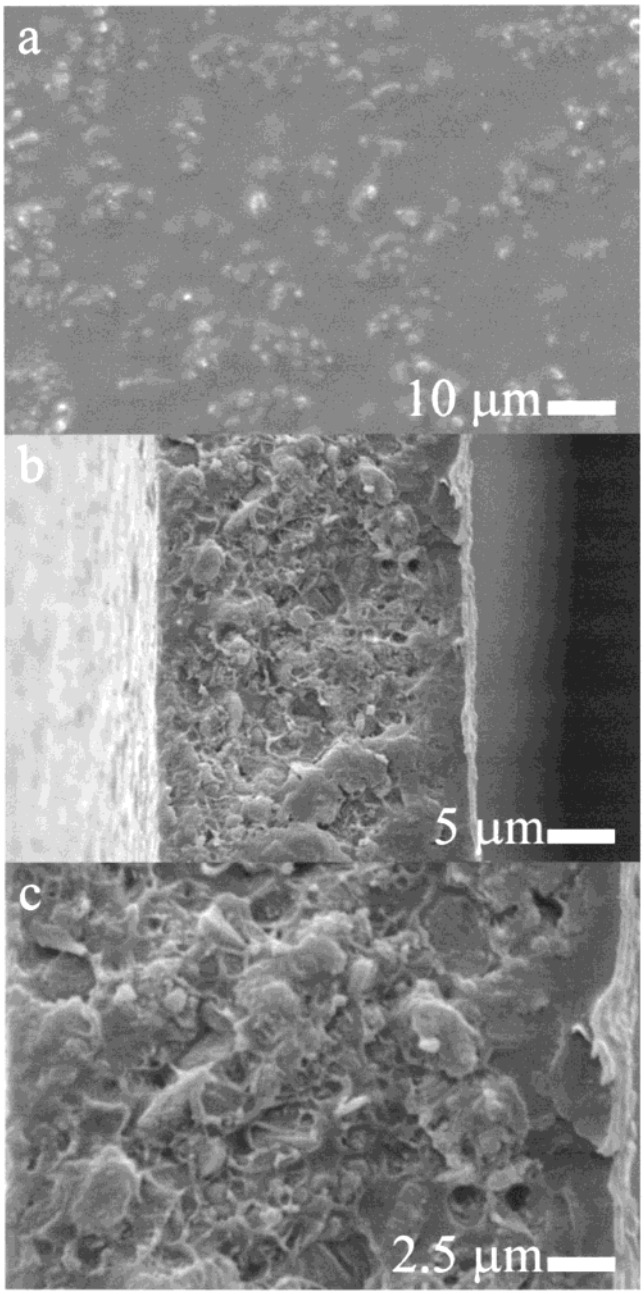

Figure 5. SEM images of a 30% (w/w) MCM-41/PSF composite membrane: (a) top down perspective; (b) cross section; (c) magnified cross section.

branes. Variations in total dissolved solids for the casting solutions resulted in slight differences in the thickness measured for each composite membrane. For the 10% composite (31.8 μm thick), the MCM-41 particles appear to be submerged under the PSF surface (Figure 3a). In the 20% composite (23.3 μm thick), a few of the MCM-41 particles appear to protrude slightly so that they are partially exposed on the top surface of the membrane (Figure 4a). Figure 5a reveals that the density of these surface-exposed MCM-41 particles in the 30% membrane (24.5 μm thick) is markedly increased in comparison with that in the 20% membrane. Cross section images of all the composite membranes revealed a jagged and irregular internal morphology characteristic of the mixed-matrix material (Figures 3b−c, 4b−c, and 5b−c). Careful inspection of the cross section images reveals that the observed roughness results from both protruding MCM-41 particles and empty cavities of similar size and shape. It is likely that these cavities represent replicas of MCM-41 particles cleaved away during the freeze-fracturing process. Composite membranes of PES with zeolites X and A have previously been reported.[12] SEM images of zeolite X/PES and zeolite A/PES composite membranes reveal the presence of porous cavities surrounding the zeolite crystals, which suggests that the polymer does not wet the zeolite surface or penetrate the zeolite pores. In contrast, the MCM-41/PSF composite SEM images at the same magnification do not show any such porous cavities surrounding MCM-41 particles. Also, the MCM-41 particles appear to be evenly distributed throughout the membranes. From the analysis of the MCM-41/PSF SEM images, it is evident that the use of mesoporous MCM-41 affords better wetting and dispersion than

Table 1. Measured Permeabilities (Barrers) of Various Gases in PSF and MCM-41/PSF Composite Membranes

membrane	MCM-41 % (w/w)	O_2	N_2	CO_2	CH_4
PSF	0	1.50 ± 0.07[a] (3)[b]	0.257 ± 0.036 (2)	7.53 ± 2.07 (2)	0.389 ± 0.008 (2)
PSF[c]	0	1.4	0.25	5.6	0.26
MCM-41/PSF	10	1.79 ± 0.10 (6)	0.354 ± 0.010 (5)	10.5 ± 0.9 (2)	0.586 (1)
MCM-41/PSF	20	2.16 ± 0.01 (10)	0.395 ± 0.014 (5)	11.4 ± 1.8 (2)	0.603 (1)
MCM-41/PSF	30	3.83 ± 0.02 (3)	0.753 ± 0.11 (4)	20.5 ± 0.9 (2)	1.05 ± 0.09 (2)
silica/PSF	10% silica	1.36 ± 0.14 (3)	0.23 ± 0.05 (3)	7.72 ± 0.9 (3)	0.16 ± 0.08 (3)

[a] 95% confidence limits. [b] () number of runs. [c] Reference 16.

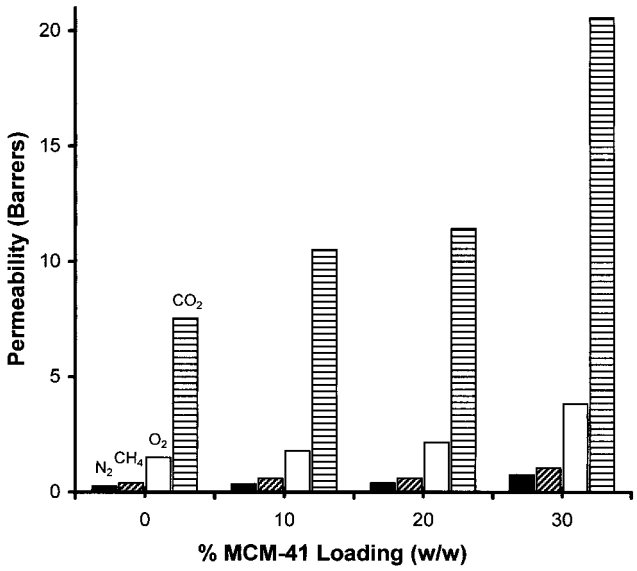

Figure 6. Effect of MCM-41 on the permeabilities of O_2, N_2, CO_2, and CH_4 for PSF membranes.

Table 2. Calculated Ideal Selectivity Factors for Selected Gas Pairs

membrane	MCM-41 % (w/w)	O_2/N_2	CO_2/CH_4
PSF	0	5.84	19.4
MCM-41/PSF	10	5.06	17.9
MCM-41/PSF	20	5.47	18.9
MCM-41/PSF	30	5.08	19.6

observed previously for PES/zeolite composite membranes.

Single Gas Permeabilities. The measured permeabilities (O_2, N_2, CO_2, CH_4) and the calculated ideal selectivity factors (O_2/N_2, CO_2/CH_4) for the pure PSF and MCM-41/PSF composite membranes are provided in Tables 1 and 2, respectively. For the gases tested, the permeability values increased in proportion to the amount of MCM-41 present in the film (Figure 6), whereas the selectivity factors decreased slightly or remained unchanged.

Addition of 30% (w/w) MCM-41 to PSF resulted in a 155% increase in the permeability of O_2 (1.50 to 3.83 Barrers) (Figure 6, Table 1). Similarly, the permeability of N_2 increased by 192% (0.257 to 0.753 Barrers) (Figure 6, Table 1). Despite these marked increases in permeability, only a moderate decrease in O_2/N_2 selectivity was observed (O_2/N_2 selectivity decreased from 5.84 to 5.08) (Table 2). Addition of 30% (w/w) MCM-41 to PSF resulted in a 172% increase in the permeability of CO_2 (7.53 to 20.5 Barrers) (Figure 6, Table 1). Similarly, the permeability of CH_4 increased by 169% upon addition of 30% (w/w) MCM-41 (0.389 to 1.05 Barrers). Despite these marked increases in permeability, CO_2/CH_4 selectivity remained virtually unchanged.

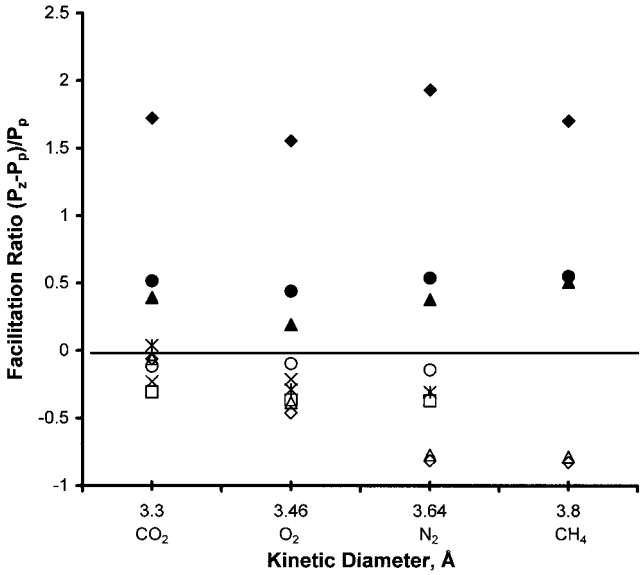

Figure 7. Facilitation plot of measured gases for MCM-41/PSF membranes compared with similar composite membranes: (○) 16% 4A/PES; (×) 33% 4A/PES; (□) 16% 13X/PES; (∗) 33% 13X/PES; (◇) 10% 13X/PSF; (△) 20% 13X/PSF; (▲) 10% MCM-41/PSF; (●) 20% MCM-41/PSF; (◆) 30% MCM-41/PSF.

Figure 7 shows the facilitation plot of the gases measured for zeolite A/PES (16 and 30% loading),[12] zeolite X/PES (16 and 30% loading),[12] zeolite X/PSF (10 and 20% loading)[2], and MCM-41/PSF (10, 20, and 30% loading). (The facilitation ratio is the difference in the permeabilities of the composite and the pure polymer divided by the permeability of the pure polymer.) At these loadings, the microporous zeolites essentially act as fillers. It was suggested that the decrease in permeability observed for zeolite A/PES and zeolite X/PES results from the condition that the penetrant gas must pass through several polymer-void interfaces with the zeolites as it permeates through the membrane.[12] It was noted that, at higher loadings, a channel network might form which connects separated voids and allows for the rapid permeation of all gases. These trends are consistent with recent results obtained for zeolite NaY/poly(3-octylthiophene) composites in which lower loadings (<20% w/w) yield a negative facilitation ratio while higher loadings result in an increased permeability for all gases tested.[17] In contrast, MCM-41/PSF composites exhibit an immediate increase in permeability with adsorbent loading of 10% or greater. For MCM-41/PSF, the monotonic increase in permeability could be a consequence of the presence of mesopores within the MCM-41 framework rather than voids at the polymer/

(16) McHattie, J. S.; Koros, W. J.; Paul, D. R. *Polymer* **1991**, *32*, 840.

(17) Madhugiri, S. M.S. Thesis, University of Texas at Dallas, Richardson, TX, unpublished.

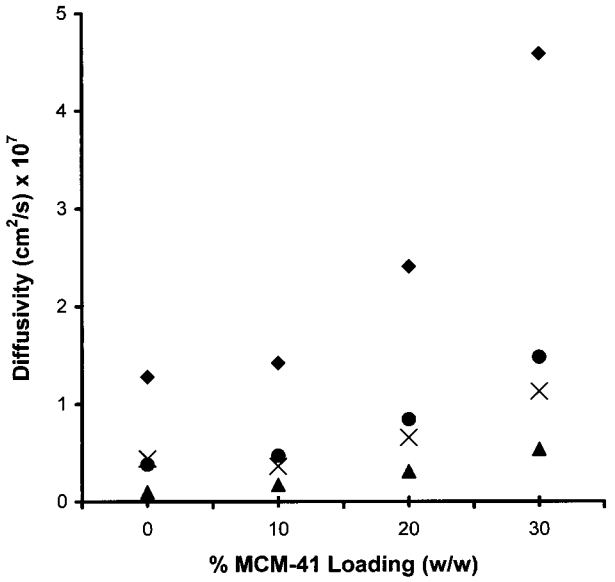

Figure 8. Effect of MCM-41 loading on the calculated diffusivities for PSF membranes: (●) CO_2; (◆) O_2; (×) N_2; (▲) CH_4.

Table 3. Diffusivity and Solubility Selectivities

membrane	MCM-41 % (w/w)	D_{O_2}/D_{N_2}	D_{CO_2}/D_{CH_4}	S_{O_2}/S_{N_2}	S_{CO_2}/S_{CH_4}
PSF	0	2.91	3.96	2.01	4.89
MCM-41/PSF	10	3.92	2.74	1.29	6.54
MCM-41/PSF	20	3.68	2.73	1.49	6.93
MCM-41/PSF	30	4.07	2.76	1.25	7.10

MCM-41 interface. When a penetrant gas molecule crosses over from the polymer phase into an MCM-41 pore, it should encounter less resistance to flow as it is translated through the 40 Å wide channel which is occupied by some measure of polymer.

Zeolite A/PES and zeolite X/PES show a modest increase in O_2/N_2 selectivity,[12] while zeolite X/PSF[2] and MCM-41/PSF show a slight decrease in O_2/N_2 selectivity. Insight into the mechanism for the permeability and selectivity trends may be gained from analysis of the solubility and diffusivity components. Diffusivity and solubility selectivities for each MCM-41/PSF composite membrane were calculated from the measured time-lags and permeabilities, and are presented in Table 3. For O_2/N_2, the diffusivity selectivity increases with the addition of MCM-41 in the membrane while the solubility selectivity decreases. Although the diffusivity of both gases increases with increasing MCM-41 loading (Figure 8), the diffusivity of O_2, with its smaller kinetic diameter, increases more rapidly than that of N_2, which is the likely reason that diffusivity selectivity increases. The solubility of N_2 remains virtually unchanged upon introduction of MCM-41, while the solubility of O_2 decreases slightly with increasing MCM-41 loading, causing the observed decrease in solubility selectivity. The net result is that the ideal O_2/N_2 selectivity is hardly compromised as a result of adding MCM-41 to the PSF membrane.

For CO_2/CH_4, the diffusivity selectivity decreases with addition of MCM-41 in the membrane, while the solubility selectivity increases (the inverse of the trend observed for O_2/N_2) (Table 3). Like the cases of O_2 and N_2, the diffusivities of both CO_2 and CH_4 increase with increasing MCM-41 loading (Figure 8). However, while the diffusivity increases for both gases, the difference in diffusivity between CO_2 and CH_4 is approximately the same for each MCM-41 loading. The increase in CO_2/CH_4 solubility selectivity is a consequence of the calculated decreased CH_4 solubility in the MCM-41 impregnated films. In this case, the decrease in diffusivity selectivity is offset by the increase in solubility selectivity resulting in an ideal CO_2/CH_4 selectivity which is virtually unaffected by the addition of MCM-41.

The increase in permeability, observed as a function of MCM-41 loading, is primarily a consequence of an increase in the diffusivity for each gas. This increase in penetrant diffusivity in MCM-41/PSF composite membranes may be attributed to nonselective microporous voids existing at the MCM-41/polysulfone interface, which effectively reduce the membrane thickness in proportion to the amount of MCM-41. Alternatively, PSF may not fill the mesopores of MCM-41, meaning that the permeating gas molecules encounter little resistance to flow once in the MCM-41 channels. The possibility that nonbonding interactions between MCM-41 and polysulfone could disrupt polymer−polymer interactions, thereby increasing the concentration of more amorphous (and more permeable) regions in the membrane, should also be considered.

To determine whether the observed increases in permeability were due to the presence of nonselective voids at the MCM-41/PSF interface, the effect of varying the upstream pressure was investigated. For pure PSF, O_2 and N_2 permeabilities are virtually independent of driving pressure while CO_2 permeability decreases slightly with increasing upstream pressure.[18] If such nonselective passages exist in the composite membranes, the change in pressure with respect to time on the downstream side of the membrane will be directly proportional to the driving pressure on the upstream side. In the case of a 10% MCM-41/PSF composite membrane, the O_2 permeability remained almost constant from 1.32 Barrers (1 atm) to 1.30 Barrers (3 atm), N_2 permeability increased slightly from 0.35 Barrers (1 atm) to 0.44 Barrers (3 atm), and CO_2 permeability decreased slightly from 6.52 Barrers (1 atm) to 6.33 Barrers (3 atm). These results demonstrate that the increased permeability observed as a function of MCM-41 loading is not due to the presence of nonselective micropores.

To further understand the nature of the interaction between the MCM-41 adsorbent and the PSF matrix, attenuated total reflectance Fourier transform infrared spectra (ATR-FTIR) were obtained for a pure PSF membrane and for a 30% (w/w) MCM-41/PSF composite membrane. No change in energy was observed for SO_2 stretching at 1324 or 1168 cm^{-1}, which argues against hydrogen bonding through the sulfonyl oxygens. However, the peak at 1232 cm^{-1} ("aryl-O" stretching, analogous to that observed in phenyl ether) shifted to 1239 cm^{-1} upon introduction of the MCM-41. It has been demonstrated by FTIR and pyridine adsorption that the surface of siliceous MCM-41 is lined with weakly acidic OH groups (0.79 mmol/g).[19] It is possible that there is a hydrogen-bonding interaction between the hydroxyl

(18) Chiou, J. S.; Maeda, Y.; Paul, D. R. *J. Appl. Polym. Sci.* **1987**, *33*, 1823.

groups on the external and/or internal surfaces of the MCM-41 and the aryl ether groups of PSF. To test this assertion, a PSF membrane was submerged in CF_3CH_2OH for 24 h and an ATR-FTIR spectrum was collected. Similar to the case of the MCM-41/PSF spectrum, the aryl-O stretch shifted to higher energy (from 1233 to 1235 cm^{-1}). In addition, the OH stretch for the CF_3CH_2OH shifted from 3350 to 3392 cm^{-1} upon introduction to the PSF. This dramatic shift to higher energy for the OH stretch of CF_3CH_2OH indicates a significant disruption in the hydrogen bonding of CF_3CH_2OH to itself upon introduction to the PSF. This result, along with the observation that the aryl-O stretch exhibits the same trend in the CF_3CH_2OH swelled PSF membrane as in the MCM-41/PSF composite membrane, suggests a hydrogen-bonding interaction between the phenyl oxygens of PSF and the surface hydroxyl groups of MCM-41. This hydrogen-bonding interaction between PSF and CF_3CH_2OH was modeled using PC Spartan Pro v1.0 (Wavefunction, Inc.). Phenyl ether and CF_3CH_2OH were geometry-optimized (semiempirical AM1) and placed in a reasonable arrangement for hydrogen bonding. The hydrogen-to-ether oxygen interatomic distance was then constrained to 2.0 Å, and the energy was again minimized. This procedure resulted in a slight decrease in the phenyl−oxygen bond distance (from 1.40 to 1.39 Å) and a corresponding increase in the theoretical aryl-O stretching frequency (from 1221 to 1227 cm^{-1}).

XRD of the composite membranes revealed no obvious change in PSF crystallinity upon formation of MCM-41 composites. This means that the increase in permeability is probably not the result of disruptions in polymer−polymer interactions. ATR-FTIR of the composite membranes provided some evidence for hydrogen bonding between the aryl ether groups of PSF and the surface hydroxyl groups of MCM-41 located primarily in the pores. Therefore, it would appear that the observed trends in permeability reflect diffusion of the small molecules through the MCM-41 mesopores which are at least partially filled with PSF.

While comparable results might be anticipated for dense silica/polymer composites of similar loadings, previous studies using such composites would argue that the mesopores of MCM-41 contribute favorably to the gas-transport properties of the MCM-41/PSF composites.[20,21] For example, in admixed composites of dense silica with poly(dimethyl siloxane) (PDMS), CO_2/CH_4 selectivity remained about the same upon introduction of the adsorptive additive. However, for a 28% (w/w) silica/PDMS composite, the CO_2 permeability decreased by approximately 18%.[20] Similarly, at a 40% (w/w) loading, silica/ethylene−propylene rubber (EPDM) composite membranes exhibited a slight increase in CO_2/CH_4 selectivity (from 4.3 for the pure EPDM to 4.5 for the silica/EPDM composite) accompanied by an 11% decrease in CO_2 permeability.[20]

Sol−gel-prepared polyimide/silica composites contain silica particles much smaller than the MCM-41 used in this study (50−150 nm diameter for silica particles in polyimide versus ~1 μm diameter for MCM-41 particles dispersed in PSF).[21] Despite the significantly smaller silica particle sizes, polyimide/silica composites exhibit higher permeability than the polymer alone (P_{CO_2}(polyimide) = 0.8, P_{CO_2}(20% silica/polyimide composite) = 2.03 Barrers) but significantly decreased selectivity (CO_2/CH_4(polyimide) = 40, CO_2/CH_4(20% silica/polyimide composite) = 25).

Similar trends were observed experimentally for a PSF composite containing dense silica (10% w/w) (Table 1). Since dense silica is compositionally similar to MCM-41 but structurally different (i.e. completely amorphous), it can help to illustrate the effect of the mesopores on the permeability properties of the MCM-41/PSF composites. For O_2, N_2, and CO_2, no statistically significant change in permeability was observed when compared to the case of pure PSF. The CH_4 permeability decreased slightly in the silica/PSF composite compared to pure PSF. Thus, in the absence of mesopores, the silica simply behaves as a filler—*decreasing* permeability without having any effect on selectivity. Conversely, for MCM-41/PSF composites, the mesopores have the effect of *increasing* permeability in direct proportion to their concentration in the film.

Conclusions

The evidence for hydrogen-bonding interactions between PSF and MCM-41, along with the observation that O_2 and N_2 permeabilities remain virtually constant when the upstream pressure is varied, demonstrates that the observed increases in permeability as a function of MCM-41 loading cannot be ascribed to the presence of nonselective voids at the MCM-41/PSF interface. This represents a significant improvement in compatibility over that of previously reported composites of this type. The increases in permeability are likely attributable to a reduced resistance to gas flow inside the large channels of MCM-41.

Mesoporous materials offer the favorable effect of dramatically increasing the permeability of the composite over that of PSF. The hydroxyl groups, which decorate the internal surface of MCM-41, provide the necessary functionality for hydrogen bonding, while the 40 Å pore size is large enough to readily enable penetration of the polymer. Together, these attributes make MCM-41 an attractive additive for universally enhancing the gas permeability of PSF without sacrificing selectivity.

This is the first report of the film-forming properties and gas-transport properties of an admixed composite of a *mesoporous* silica molecular sieve with a polymer. It is clear that no strong interaction exists between the MCM-41 and the penetrant gases, since virtually no change in selectivity was observed. However, the marked enhancement in permeability, along with the microscopic and spectroscopic evidence for favorable MCM-41/PSF interactions, makes further work with this system promising. Efforts are currently underway to enhance the MCM-41/penetrant gas interaction via functionalization of the channel walls and subsequent

(19) Jentys, A.; Kleestorfer, K.; Vinek, H. *Microporous Mesoporous Mater.* **1999**, *27*, 321.
(20) Duval, J. M.; Folkers, B.; Mulder, M. H. V.; Desgrandchamps, G.; Smolders, C. A. *J. Membr. Sci.* **1993**, *80*, 189.
(21) Joly, C.; Smaihi, M.; Porcar, L.; Noble, R. D. *Chem. Mater.* **1999**, *11*, 2331.

metal complexation in order to effect facilitated transport of penetrant gases.[22] Other selectivity-enhancing permutations with this system might include MCM-41 morphology control and isomorphous framework substitution with metal ions.[23]

(22) Diaz, J. F.; Balkus, K. J., Jr.; Bedioui, F.; Kurshev, V.; Kevan, L. *Chem. Mater.* **1997**, *9*, 61.
(23) Ciesla, U.; Schuth, F. *Microporous Mesoporous Mater.* **1999**, *27*, 131.

Acknowledgment. This material is based in part upon work supported by the Texas Advanced Technology Program under Grant No. 009741-0058-1997. Financial support from the Mobil Technology Company and from the U.S. Department of Energy Pittsburgh Energy Technology Center under Grant No. DE-FG22-94PC94222 is also gratefully acknowledged.

CM000931+